Kinetics of CO_2 Absorption by Aqueous 3-(Methylamino)propylamine Solutions: Experimental Results and Modeling

Juliana G. M.-S. Monteiro, Saddam Hussain, Hammad Majeed, Emmanuel O. Mba, Ardi Hartono, Hanna Knuutila, and Hallvard F. Svendsen

Dept. of Chemical Engineering, Norwegian University of Science and Technology, N-7491 Trondheim, Norway

DOI 10.1002/aic.14546

Published online July 9, 2014 in Wiley Online Library (wileyonlinelibrary.com)

Experimental data and a model for the initial kinetics of CO_2 into 3-(methylamino)propylamine (MAPA) solutions are presented in work. MAPA has been tested as an activator for tertiary amines with encouraging results. The measurements were performed in a string of discs contactor and, as no initial kinetics data are available in literature, additional measurements were carried out and in a wetted wall column. The obtained overall mass-transfer coefficients from both apparatuses are in reasonable agreement. To obtain values for the observed kinetic constant, k_{obs}, the experimental results were interpreted using a two-film mass-transfer model and invoking the pseudo-first order assumption. Needed experimental values for density, viscosity, and Henry's law coefficient for CO_2 were measured and are given. The results indicate that MAPA is almost twice as fast as piperazine, eight times faster than 2-(2-aminoethyl-amino)ethanol (AEEA), and 15 times faster than monoethanolamine, when comparing unloaded 1 M solutions at 25°C. The observed kinetic constant was modeled using the direct mechanism. The final expression for k_{obs} can be applied for any concentration and temperature within the experimental data range, and, together with the presented physical data, comprises a complete model for calculating absorption fluxes. © 2014 American Institute of Chemical Engineers AIChE J*, 60: 3792–3803, 2014*

Keywords: absorption, reaction kinetics, gas purification, mathematical modeling, mass transfer

Introduction

An ideal amine for CO_2 absorption should combine fast kinetics, reasonable heat of absorption, and high equilibrium temperature sensitivity, all potentially reducing the regeneration energy requirement and absorber size. Typically, the aim is a solvent that gives an optimal trade-off between fast kinetics and low energy requirements. One possibility is blending carbamate formers, primary or secondary amines (activators), with tertiary or sterically hindered amines which would preferentially give bicarbonate formation and, thus, possibly lower the energy demand for regeneration.

This work presents new experimental data and a model for the initial kinetics of CO_2 into 3-(methylamino)propylamine (MAPA) solutions. MAPA is a diamine with one primary and one secondary group, and it has been shown that the CO_2 absorption rates into 8 M MAPA at low CO_2 partial pressures are higher than for 8 M monoethanolamine (MEA).[1] Screening tests performed by Brúder and Svendsen[2] at 40°C and below 10 kPa CO_2 partial pressure indicate that the initial absorption rate of 5 M MAPA is higher than that of 5 M MEA, and this difference increases with loading. Additionally, loadings as high as 5 mol CO_2/kg of solution were obtained.[2] MAPA has been tested as an activator for dimethyl-monoethanolamine,[3] *N*,*N*-diethylethanolamine,[4] 2-amino-2-methyl-1-propanol,[5] triethylamine, and *N*,*N*-dimethylbutylamine[6] with encouraging results.

Correspondence concerning this article should be addressed to H. F. Svendsen at hallvard.svendsen@chemeng.ntnu.no.

Measurements

Chemicals

MAPA (CAS number: 6291-84-5) was obtained from Sigma Aldrich with purity ≥98%, while the gases were supplied by AGA Gas GmbH and Yara with purity ≥99,99 mol % for CO_2 and ≥99,999 mol % for N_2. MAPA solutions were prepared by weighing in and mixing the solvent with deionised water (DI) at room temperature.

Kinetics

A string of discs contactor was used for studying the reactive absorption of CO_2 into liquid MAPA solutions. This type of apparatus was first described by Stephens and Morris[7] as a suitable apparatus for determining absorption coefficients experimentally. The string of discs column (SDC) used in this work has 43 discs of 4 mm thickness and 1.5 cm diameter, leading to a column length of 64.5 cm and a total mass transfer area of 0.0219 m^2. The apparatus, previously described by Ma'mun et al.,[8] Knuutila et al.,[9] and Hartono and Svendsen,[10] among others, promotes the contact of a gas stream (a mixture of N_2 and CO_2) and a liquid solution in counter-current mode. Figure 1 shows the experimental setup of the SDC apparatus.

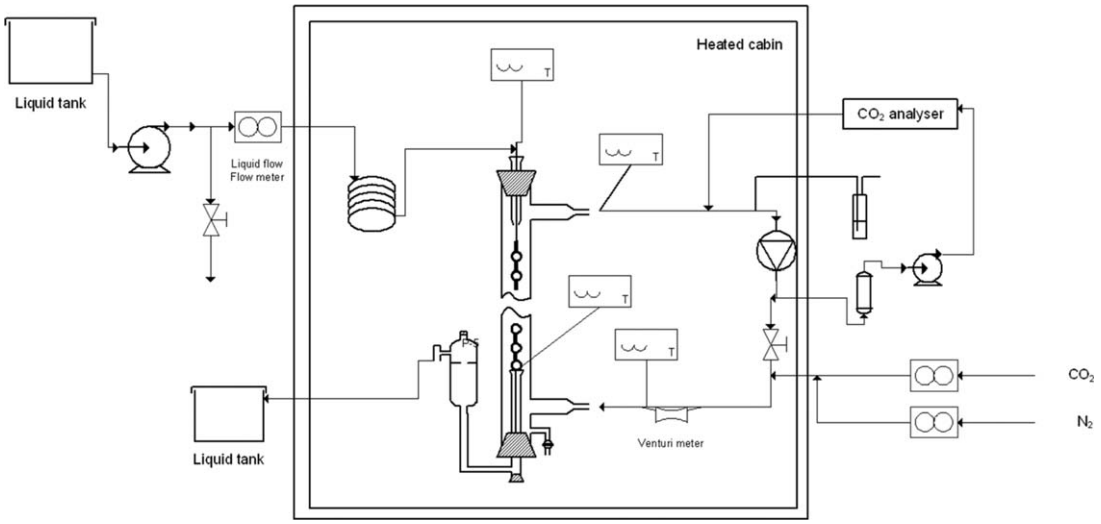

Figure 1. Experimental setup of the SDC apparatus.[9]

The inlet flow rates of N_2 and CO_2 were set using mass flow controllers with uncertainty less than 1% of measured flow, while the CO_2 composition in the outlet gas was determined by an IR CO_2 analyzer. The analyzer was calibrated every day, before the measurements were made, and the accuracy in the readings was 0.01%. The gas was circulated in the system with a flow rate of approximately 3 m^3/h, while the liquid flow was once through and the rate was kept constant at approximately 50 mL/min. The operation was carried out at ambient pressure and pressure indicators for the gas inlet and outlet streams determined the pressure drop along the column.

The column is enclosed in an insulated heating chamber and the experiments were performed in the temperature range 25 to 62°C. An experimental point was considered stable when the temperatures of the gas and liquid streams at the top and bottom of the column, as well as the gas composition, showed constant values for at least 5 min. The calculations considered the averages of 2 min online readings, and the standard deviations in the measurements within this period were used for uncertainty evaluations.

The experiments were conducted for unloaded aqueous solutions of MAPA at the following concentrations: 1 M (9 wt %), 2 M (18 wt %), 3 M (27 wt %), 4 M (36 wt %), and 5 M (45 wt %). The end solutions were analyzed for total alkalinity and CO_2 content. All analyses indicated no measurable variation in the amine content of the solutions. The final loadings were always smaller than 0.01 mol CO_2/mol MAPA.

Because there is no data available in the literature for the kinetics of unloaded MAPA solutions, extra measurements for the 2 M MAPA solution were performed in a wetted wall column (WWC). The apparatus and the experimental procedures are described in detail by Luo et al.,[11] who showed that the measurements performed in the two apparatuses are consistent.

Physical properties

To interpret the results obtained in the SDC experiments, it was necessary to determine the following physical properties of the solutions: density, viscosity, Henry's constant, and diffusivity of CO_2. The two first properties were measured directly. Henry's law constant of CO_2 was calculated from measurements of Henry's constant of N_2O in the solution using the N_2O analogy.[12] The diffusivity of CO_2 in the solution was estimated using the correlations given by Versteeg et al.[13]

The viscosities of the MAPA solutions were determined using an Anton Paar Rheometer Physica MCR 100, with the DG 26.7 measuring system and the TEK 150P-C measuring cell. Series of repeated measurements indicated that the uncertainty of the viscosity measurements is around $\pm 2\%$ for the viscometer used in this work.[14] The experimental results from 20 to 80°C are given in Table 1.

The densities were measured using an Anton Paar Stabinger Density Meter DMA 4500. Nominal repeatability is of 10^{-5} g/cm^3 for density and 0.01°C for temperature. Series of repeated measurements indicated that the uncertainty of the density measurements was $\pm 3 \times 10^{-5}$ g/cm^3.[15] The experimental results from 20 to 70°C are given in Table 2.These results are in good agreement with those obtained by Pinto et al.[15]

The N_2O solubility apparatus used and the calculation procedure for determining Henry's constant of N_2O are described in detail by Knuutila et al.[16] The measurements were carried out from 25 to 65°C. The results are given in Table 3. The uncertainty of the measured N_2O solubilities is estimated to be $\pm 7.5\%$.

Calculation of the pseudo-first order kinetic constant

From the performed experiments in both the SDC and the WWC, the CO_2 absorption flux is determined by a mass

Table 1. Viscosity Data for MAPA Solutions, mPa s

T (°C)	1 M	2 M	3 M	4 M	5 M
20	1.598	2.527	4.353	7.655	13.057
25	1.397	2.135	3.566	6.037	9.944
30	1.234	1.834	2.977	4.875	7.729
40	0.981	1.402	2.164	3.332	4.974
50	0.808	1.120	1.649	2.416	3.364
60	0.702	0.921	1.311	1.833	2.362
70	0.601	0.778	1.072	1.437	1.774
80	0.503	0.647	0.870	1.159	1.361

Table 2. Density Data for MAPA Solutions, g cm^{-3}

T (°C)	1 M	2 M	3 M	4 M	5 M
20	0.99221	0.98854	0.98647	0.98438	0.97873
30	0.98914	0.98445	0.98098	0.97742	0.97077
40	0.98522	0.97963	0.97499	0.97018	0.96257
50	0.98047	0.97428	0.96854	0.96269	0.95425
60	0.97541	0.96836	0.96176	0.95496	0.94585
70	0.96966	0.96198	0.95458	0.947	0.93718

balance (Eq. 1). The inlet CO_2 and N_2 fluxes were measured directly by mass flow. A side stream of the circulating gas is analyzed online for CO_2 using an IR analyzer. Prior to the analysis, the gas is cooled down to 20°C to avoid water condensation in the analyzer. The condensate is separated and the dry gas passes to the analyzer (see Figure 1). The CO_2 outlet flux can be calculated from Eq. 2. In this equation, $y_{CO_2,out}$ is the mol fraction of the dried gas, as read from the analyzer and $N_{N_2,out}=N_{N_2,in}$ is the small but constant flow of inert through the apparatus

$$N_{CO_2}=N_{CO_2,in}-N_{CO_2,out}=N_{N_2,in}\left(y_{CO_2,in}-y_{CO_2,out}\right) \quad (1)$$

$$N_{CO_2,out}=N_{N_2,in}\frac{y_{CO_2,out}}{1-y_{CO_2,out}} \quad (2)$$

The overall mass-transfer coefficient can be calculated as the ratio between the CO_2 absorption flux and the driving force (Eq. 3). As the experiments reported in this work comprise only unloaded solutions, the logarithmic mean of the CO_2 partial pressure difference in the inlet and outlet streams was calculated using Eq. 4

$$K_{ov}=\frac{N_{CO_2}}{\Delta p^{LM}_{CO_2}} \quad (3)$$

$$\Delta p^{LM}_{CO_2}=\frac{P_{CO_2,out}-P_{CO_2,in}}{\ln\left(\frac{P_{CO_2,out}}{P_{CO_2,in}}\right)}\cong\frac{P_{CO_2,out}+P_{CO_2,in}}{2} \quad (4)$$

By applying the two-film theory,[17] the overall mass-transfer coefficient can be split into a gas- and a liquid-side mass-transfer coefficient, as shown in Eq. 5. Given that the reaction takes place in the pseudo-first order regime ($Ha \geq 3$ and $E \ll E_\infty$), the enhancement factor is equal to the Hatta number and given by Eq. 6.16[17] Hence, the pseudo-first order kinetic constant can be calculated from Eqs. 5–7

$$K_{ov}=\frac{1}{\frac{1}{k_G}+\frac{H_{CO_2}}{Ek^0_L}}=\frac{1}{\frac{1}{k_G}+\frac{H_{CO_2}}{k_L}} \quad (5)$$

$$E=Ha=\frac{\sqrt{k_{obs}D_{CO_2}}}{k^0_L} \quad (6)$$

$$k_{obs}=\frac{H^2_{CO_2}}{\left(\frac{1}{K_{ov}}-\frac{1}{k_G}\right)^2 D_{CO_2}} \quad (7)$$

The gas film mass-transfer coefficient, k_G, and the liquid film physical mass-transfer coefficient, k^0_L, are dependent on the gas and liquid flow properties, respectively, as well as the apparatus geometry, and were calculated using the correlations given by Ma'mun et al.[8] for this SDC.

Uncertainty evaluation

The measurements were saved in a log file every 10 s. When the experiment reached a stable condition, a point was taken by averaging the logged values over 2 min (i.e., considering 12 log entries). This should be a large enough number to provide a reliable standard deviation.[18] Hence, if x is a measured quantity, the value used in the calculations was its average ($\bar{x}$, given by Eq. 8), and the measurement uncertainty, u_x, was given by its standard deviation (Eq. 9), as the uncertainties are considered to have a normal distribution

$$\bar{x}=\frac{1}{12}\sum_{i=1}^{12}x_i \quad (8)$$

$$u_x=\sqrt{\frac{1}{11}\sum_{i=1}^{12}\left(x_i-\bar{x}\right)^2} \quad (9)$$

The propagation of these uncertainties will reflect on the uncertainty of the calculated variables, such as K_{ov} and k_{obs}. Given a generic calculated variable, as defined in Eq. 10, the propagation Eq. 11 is used to assess its uncertainty[18]

$$f=f(a_1,a_2,\ldots,a_n) \quad (10)$$

$$u_f=\sqrt{\sum_{k=1}^{n}\left(\frac{\delta f}{\delta a_k}\right)^2 u^2_{a_k}} \quad (11)$$

Table 3. Henry's Law Constant for N_2O in MAPA Solutions, Pa m^3 mol^{-1}

T (°C)	1 M	2 M	3 M	4 M	5 M
25	4316	4803	5674	6584	6869
35	5533	5957	6625	7354	7348
45	6822	7200	7629	8030	7650
45	6790	7131	–	8031	–
55	8345	8467	8599	8640	8003
55	–	–	8529	–	–
65	10145	10090	9719	9311	8508

Modeling of the pseudo-first order kinetic constant

Many reactions take place when CO_2 is absorbed by aqueous amine solutions. The direct reaction of CO_2 with water, Reaction 12, is negligible at high pH[9] and was, therefore, disregarded in this work. Additionally, the reaction of CO_2 with hydroxyl ion, Reaction 13, was found to be negligible (in all tested cases its contribution to the overall rate was less than 0.1%).

This indicates that the CO_2 absorption by unloaded aqueous MAPA solutions takes place mainly through the reactions of carbamate formation. The formation of MAPA carbamates can occur either on the primary or the secondary amine functionalities, and this is indicated by the subscripts p and s on the carbamate species. A simplified representation of the carbamate formation reactions is given in Reactions 14 and 15. As all the experiments in this work were performed on initially unloaded amine, the possible formation of a dicarbamate could safely be disregarded as shown by Ciftja et al.[19] The structures of the two different MAPA carbamates are given in Figure 2

$$CO_2+H_2O \leftrightarrow H_2CO_3 \quad (12)$$

$$CO_2+OH^- \leftrightarrow HCO_3^- \quad (13)$$

$$MAPA+CO_2+B \leftrightarrow MAPACOO^-_p+BH^+ \quad (14)$$

$$MAPA+CO_2+B \leftrightarrow MAPACOO^-_s+BH^+ \quad (15)$$

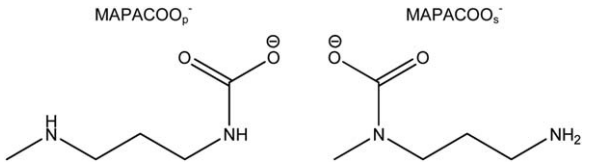

Figure 2. MAPA carbamates.

The observed reaction rate is actually the sum of the rate of formation of the two carbamate species. There is no way of differentiating the rate of formation of primary from that of secondary carbamates from the experiments performed in this work. The results of Ciftja et al.[19] indicate that already at low loadings both carbamates are present at equilibrium, and the concentration of the primary carbamate is about 3 to 4 times that of the secondary. As it would be very uncertain to apply the same ratio for initial kinetics, we have decided to consider the sum of the carbamate formation rates in our analysis.

The carbamate reactions require the presence of a base component. As mentioned earlier, the loading values throughout the experiments performed in this work were very low, practically negligible. Therefore, only MAPA and water were considered as relevant bases. Other basic species such as the formed monocarbamates are present only in very low concentrations.

There are two traditional mechanisms proposed in the literature for explaining the reaction between CO_2 and primary or secondary amines. The first mechanism suggests a two-step reaction with the formation of a zwitterion as intermediate.[20] The second mechanism proposes a direct reaction where the nitrogen atom in the amine bonds with the carbon atom in CO_2 while a proton is simultaneously transferred from the amino nitrogen to an already complexated base, water, or amine.[21]

da Silva and Svendsen[22] performed *ab initio* calculations using a continuum model and concluded that the direct mechanism is the most likely. Shim et al.[23] performed a similar study, considering a polarizable continuum, and achieved the same result. In the study presented by Arstad et al.[24] water molecules are explicitly included in the molecular model. The authors also conclude that a mechanism very similar to that proposed by Crooks and Donnellan[21] seems to take place and suggest that the transition state may be of zwitterionic nature. Based on these works, we have chosen to model the reaction according to the direct mechanism. Hence, the total rate of carbamates formation is given by Eq. 16. This expression can also be arrived at by means of the zwitterion mechanism, but in that case it would be necessary to assume that the rate of deprotonation of the zwitterion is the rate determining step, which seems unlikely

$$-r_{CO_2} = \{k_{MAPA} c_{MAPA} + k_{H_2O} c_{H_2O}\} c_{MAPA} c_{CO_2} \tag{16}$$

The pseudo-first order kinetic constant (k_{obs}) is modeled as in Eq. 17. The kinetic constants in the model were assessed using the Arrhenius deterministic relation, that is, they were unfolded into one pre-exponential (or frequency) factor, (a_i), and one energy factor, (b_i), as in Eq. 18

$$k_{obs} = \{k_{MAPA} c_{MAPA} + k_{H_2O} c_{H_2O}\} c_{MAPA} \tag{17}$$

$$k_{obs} = \left\{ a_{MAPA} \exp\left(\frac{b_{MAPA}}{T}\right) c_{MAPA} + a_{H_2O} \exp\left(\frac{b_{H_2O}}{T}\right) c_{H_2O} \right\} c_{MAPA} \tag{18}$$

The pre-exponential factor is connected to the frequency of collisions between reactants, while the energy factor is related to the activation energy through Eq. 19[25]

$$b_i = \frac{-E_{act,i}}{R} \tag{19}$$

Taking these physical meanings into consideration, the frequency factors may be dependent on the solution concentration and on the temperature. The temperature dependency of the frequency factor is actually predicted by both Collision and Transition State theories, but its influence is normally very small when compared to the exponential term.[26]

The energy factor is normally not considered to be a function of concentration nor temperature, as the activation energy depends only on the energy level of the reactants and that of the transition state complex. Hence, in this work, the frequency factor is considered a function of the concentration only, while the energy factor is independent both of concentration and temperature.

The physical meaning attributed to the frequency and the energy factors, conversely, is only valid when elementary reactions are taken into consideration (i.e., no intermediates are formed).

To understand the mechanism of CO_2 absorption into aqueous MAPA solutions, fundamental knowledge of the liquid structure, not obtainable from macroscopic kinetic studies, is needed. Molecular modeling studies on the CO_2 absorption in aqueous MEA solutions are available in literature.[22–24,27–29] Because studies with different modeling premises may come to different conclusions regarding the stability of conformers, caution should be taken when evaluating the results. For instance, Han et al.[28] indicate that, although MEA molecules may form ring structures (due to internal hydrogen bonding), the chain configuration is the most stable when water molecules are explicitly included in the model.

Amongst the different studies, there are also differences regarding which species take part in the carbamate formation reaction. While some studies[27–29] indicate that only MEA molecules act as proton receivers, the simulations performed by Arstad et al.[24] show the possibilities of both MEA and water acting as proton receivers and show that the activation energy for water is considerably higher than for MEA.

da Silva et al.[27] conclude that there is a low degree of interaction between the amine functionalities of different MEA molecules (in a 30 wt % solution), and suggest that the event of having a CO_2 molecule, a reacting MEA molecule and a second MEA molecule is relatively rare. Because the MEA carbamate formation is relatively fast, this result may suggest that another molecule—water—will act as a base.

Gupta et al. (submitted) actually address the formation of MAPA carbamates using an explicit solvation shell model. The authors simulate clusters of MAPA (or MAPA carbamate) and five water molecules and show that while the chain MAPA conformer is the most stable structure in unloaded aqueous solutions, due to strong interactions between the nitrogen atoms in MAPA and water molecules, the carbamate is more stable in a cyclic form, as shown in Figure 3. However, the mechanism of formation of the carbamate is not discussed.

None of the studies mentioned in this section provide a study on the effects of solution concentration and temperature on conformers stability. Such effects could directly influence the kinetics of carbamate formation.

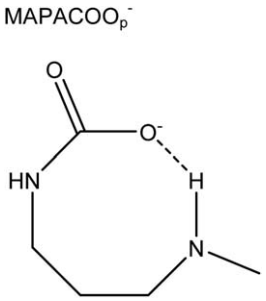

Figure 3. Cyclic MAPA carbamate.

The dotted line represents a hydrogen bond.

Results and Discussion

Pseudo-first order kinetic constant

The experimental data, physical properties, and calculation results for the transport and the pseudo-first order kinetic constants are presented in Appendix for the solutions of MAPA with concentrations varying from 1 to 5 M. It can be seen that the experiments show good reproducibility and the results obtained in 2011 do not show any systematic deviation from those obtained in 2013. Moreover, the repeatability is also good.

The SDC and the gas lines are placed inside an insulated heating chamber and the liquid solution flows through a coil before reaching the column inlet. Additionally, the gas stream is saturated prior to the column to avoid evaporation from the liquid phase. However, these measures did not guarantee equal gas and liquid inlet and outlet temperatures.

Typically, the liquid inlet and outlet temperatures departed 2°C from each other, but ΔT up to 4.6°C was observed in the low concentration, high temperature range. Normally the liquid inlet temperatures were lower than the outlet temperatures and the difference can be a consequence of the heat of reaction. The gas inlet temperatures were normally 2°C higher than the outlet, and up to 4°C higher than the liquid inlet. The higher gas temperatures can be due to the heat generated by the gas fan upstream the gas inlet temperature measurement.

Therefore, the temperatures presented in Appendix are the averages of the liquid inlet and outlet readings. This is believed to give the best representation of the temperature at which the CO_2 absorption takes place in each experiment.

The physical properties presented in Appendix are calculated for the actual experimental solution concentration and temperature based on the values given in this work by bilinear interpolation.

The calculated overall mass-transfer coefficients are shown in Figure 4. As previously observed for the CO_2 absorption by other amines at approximately the same temperature range,[11,30,31] they increase with increasing temperature and also show a strong dependency on the solution concentration.

Because the absorption reaction is exothermic (and, therefore, less favored at higher temperatures), and as the gas solubility decreases with temperature, the observed increase of the overall mass-transfer coefficient with temperature can only be due to the temperature effect on the reaction kinetics.

Moreover, Kim[32] has shown that the heat of absorption of CO_2 in 8 wt % MAPA (~1 M) increases from around −85 kJ/mol at 40°C to −90 kJ/mol at 80°C in the low loading region. Hence, at the experimental range of the kinetics experiments (25 to 60°C), this effect is nearly negligible.

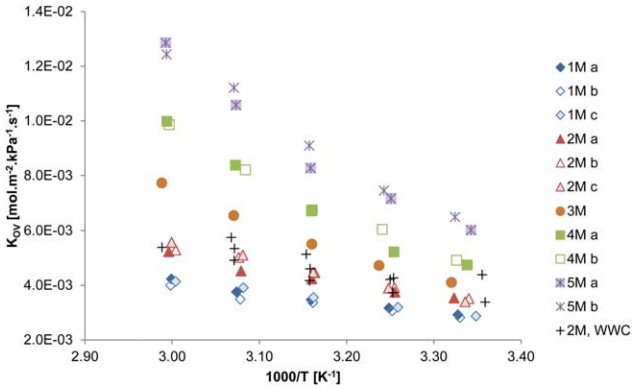

Figure 4. Calculated values for K_{ov} as a function of temperature.

[Color figure can be viewed in the online issue, which is available at wileyonlinelibrary.com.]

There is a reasonably good agreement between the data obtained in the SDC (triangles) and in the WWC (crosses) for the 2 M MAPA solution. However, because no uncertainty analysis was performed for the data obtained in the WWC, those were not included in the parameter fitting procedure.

The pseudo-first order kinetic constant (k_{obs}) shows a reasonably linear behavior in the Arrhenius diagram (Figure 5), especially for concentrations up to 3 M. Changes in the slope can be either an indication of a shift in the controlling reaction mechanism[33] or a consequence of experimental errors. If the data are believed to be correct, as the good agreement between parallel measurements suggests, then, from Eq. 17, the changes in the slopes are results of a physical change in the roles of MAPA and water as proton receivers. As aforementioned, the kinetic data represent the sum of carbamate formation both on the primary and secondary amine groups. These cannot be distinguished, and a shift from, for example, predominantly a primary carbamate formation to more secondary carbamate formation, may explain the change in slope.

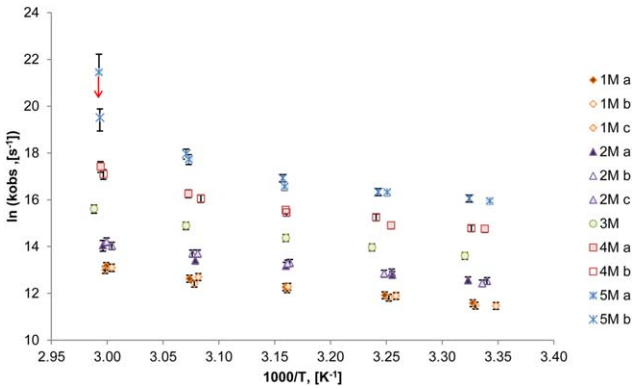

Figure 5. Arrhenius plot of k_{obs}.

The uncertainty for the 5 M a run at 61°C was greater than 100%. Due to the logarithmic plot, the negative error bar cannot be properly represented. A red arrow is included to graphically indicate this. [Color figure can be viewed in the online issue, which is available at wileyonlinelibrary.com.]

The calculated uncertainties in the K_{ov} measurements, as defined in 3.1, were in this work found to be around 1%. From Figure 5, it can be seen that the actual variability in the data is greater than 1%, and the practical repeatability of K_{ov} is about 5%. This means that error sources that are not computed, such as random experimental errors, are the main contributors to the observed variability in K_{ov}.

As density and viscosity data are reasonably accurate, and given that the dependency of the observed first order kinetic constant to these properties is not high, these measurements do not contribute significantly to the uncertainty in k_{obs}. Apart from the uncertainty in K_{ov}, another major source of uncertainty in the k_{obs} calculations comes from the solubility data. Given that the Henry constant's uncertainty could be estimated to $\pm 7.5\%$, it follows that the uncertainty in k_{obs} will be at least 15% (as k_{obs} is proportional to the square of the Henry's constant).

The experimental procedure used is based on steady state stable levels of CO_2 in the gas circulation loop. The experiments performed at high MAPA concentrations and temperatures show significantly more unstable readings for the gas phase CO_2 concentration than for other conditions. For that reason, the points for 4 M (runs a and b) at 61°C and 5 M (runs a and b) at 52°C have uncertainties of at least 20%; while the points for 5 M at 61°C have uncertainties of at least 110% (run a) and 44% (run b). The value obtained in "run a" for 5 M MAPA solution at 61°C is, therefore, not reliable at all, and was only included in this work to illustrate the influence of the fluctuations in the readings on the obtained results, as well as to stress the importance of evaluating the data uncertainties and considering such information when modeling.

In the uncertainty analysis, some simplifying assumptions had to be made. For instance, the correlation for determining k_G was considered to be exact, as well as the relationship between MAPA diffusivity in the solution and the solution viscosity. However, the obtained values for the uncertainties are considered to be a good approximation of the real values and are, therefore, taken into consideration in the parameter regression.

Parameter regression

The expressions obtained by applying the direct mechanism to describe carbamate formation are summations of exponentials, as in Eq. 12. Applying a logarithmic transformation to this form of equations would result in polynomials in $1/T$ with an order determined by the number of terms in the summation. Therefore, the logarithmic transformation of Eq. 18 would result in a second order polynomial. However, if only one base is considered, the transformation results is a linear function in $1/T$, and the parameters can be obtained by linear regression.

Literature provides an interesting debate on the regression of the Arrhenius equation parameters. While Brauner and Shacham,[34] Curl,[35] and Sundberg[36] defend the linearization of the equation, Schwaab and Pinto,[26] Chen and Aris,[37] and Klicka and Kubácek[38] argue against it. According to Schwaab and Pinto,[26] the logarithmic transformation of the Arrhenius equation is better avoided because it is otherwise difficult to keep the error structure of the experimental observations.

To avoid controversial and cumbersome statistical treatment of the kinetic constants and respective uncertainties, in this work we chose to follow the approach of Schwaab and Pinto[26] and inserted the Arrhenius equation into the kinetic rate expressions, Eq. 18, and used the heuristic particle swarm optimization (PSO) algorithm[39] to perform a nonlinear regression and provide both the parameter estimates and a statistical evaluation of the joint confidence regions. Schwaab et al.[40] show that the confidence regions of kinetic constants can be very complex, showing nonconvexity and being constituted by disconnected regions.

The PSO algorithm does not require initial guesses for the model parameters and does not use derivatives. It was implemented using the local best topology and the tuned PSO parameter values presented by Poli et al.[41] Details of the implementation of the PSO method are given elsewhere.[42]

The parameter regression problem is formulated as a minimization of the squared difference between the experimental and the modeled value of the pseudo-first order kinetic constant, weighed using the estimated uncertainties. The variables' transformations presented in Eqs. 20 and 21 were used to avoid numeric precision issues connected to very high values of the pre-exponential terms. The final formulation is presented in Eq. 22

$$\alpha_{MAPA} = \ln a_{MAPA} \tag{20}$$

$$\alpha_{H_2O} = \ln a_{H_2O} \tag{21}$$

$$F_{obj}(j) = \sum_{i=1}^{NP(j)} \frac{\left(k_{obs}(i,j) - \left\{ \begin{array}{l} \exp\left(\alpha_{MAPA} + \dfrac{b_{MAPA}}{T}\right) c_{MAPA}(i,j) + \\ \exp\left(\alpha_{H_2O} + \dfrac{b_{H_2O}}{T}\right) c_{H_2O}(i,j) \end{array} \right\} c_{MAPA}(i,j) \right)^2}{u^2_{kobs}(i,j)} \tag{22}$$

The optimization was performed in two steps. Initially, 12 parameters were fitted using all the experimental data available: two energy parameters, b_{MAPA} and b_{H2O}, which are the same regardless of the solution concentration, and 10 pre-exponential parameters, α_{MAPA} and α_{H2O}, (i.e., two per solution concentration). In the second step, the optimized energy parameters were kept constant and five optimizations were carried out, one for each concentration. This reduces the problem to be solved, as only two parameters are fitted and the number of experimental points available varies from 5 to 15 per solution concentration.

The optimization results are presented in Table 4. Using Eq. 19, the activation energies obtained are 39 kJ/mol for MAPA and 182 kJ/mol for water, respectively. The value obtained for MAPA is similar to those obtained by Ma'mun et al.[8] and Bishnoi and Rochelle[31] for AEEA and piperazine (PZ), respectively. The value obtained for water is very high, and although it could be argued that Arstad et al.[24] predicts high activation energy for the MEA carbamate

Table 4. Optimization Results

MAPA Concentration	F_{obj}	ARD %	α_{MAPA}	a_{MAPA}	b_{MAPA}	α_{H_2O}	a_{H_2O}	b_{H_2O}
1 M	7.8	8.4	13.58	793,731	−4792	58.87	3.69E+25	−22365
2 M	6.8	7.3	13.19	534,774	−4792	60.12	1.28E+26	−22365
3 M	0.02	0.8	13.47	710,838	−4792	62.92	2.12E+27	−22365
4 M	4.3	9.3	14.02	1,229,355	−4792	65.00	1.69E+28	−22365
5 M	10.6	23.5	14.80	2,674,572	−4792	66.98	1.23E+29	−22365

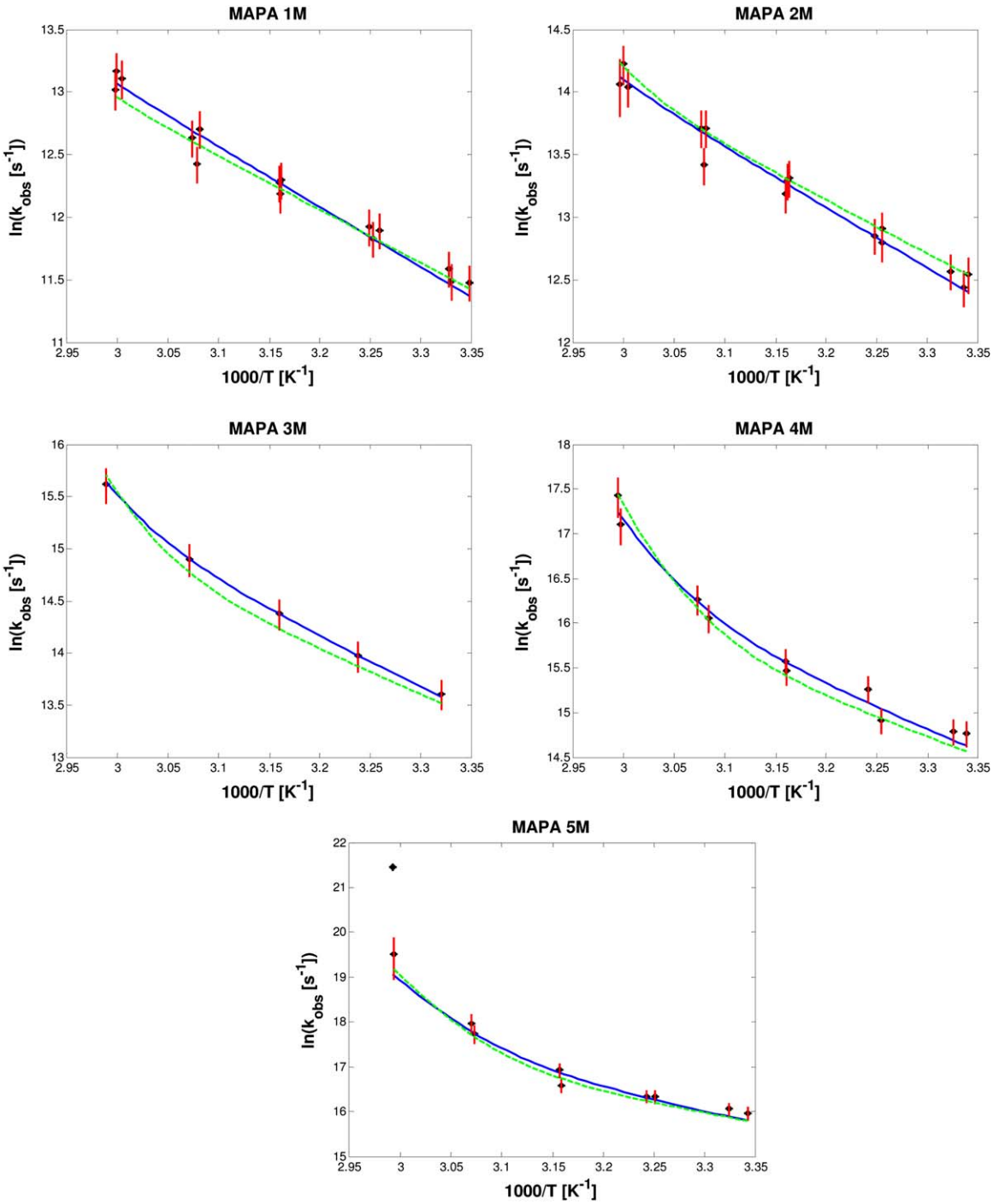

Figure 6. Arrhenius plots showing the optimization results.

Black points: experimental points presented in this work. Red vertical lines: error bars. Blue lines: fitted model using Eq. 22. Green lines: fitted models using Eq. 27. [Color figure can be viewed in the online issue, which is available at wileyonlinelibrary.com.]

formation when water is the proton receiver, this result should be interpreted with care as such a high number may be a mathematical artefact to allow the proposed model to fit the experimental data. The model adopted in this work is relatively simple and does not account for possible changes in the solution structure with temperature and concentration. One may speculate that at low temperature and high MAPA concentration, the ring structure predicted by Gupta et al. (submitted) is stable, resulting in the dominating effect of MAPA as base (it is assumed that while one nitrogen of the MAPA molecule reacts with CO_2, the second nitrogen is close enough to act as a base, forming a zwitterion as a transition species). At low MAPA concentrations and higher temperatures, the ring structure may become less stable leading to a stronger effect of water as base. Thus, relatively speaking, the effect of water could increase significantly, and this may at least partly explain the high apparent activation energy obtained. However, directly inferring the mechanistic behavior from the results presented herein may be stretching the obtained model beyond its possibilities.

The goodness of the fit can be evaluated from the average relative deviation, defined in Eq. 23, as well as from the plots presented in Figure 6. The somewhat high ARD for MAPA 5 M is due to the point at 60°C, run a. As the uncertainties are taken into consideration in the objective function, the obtained minimum value is comparable to that obtained for 1 M

$$\mathrm{ARD}=\frac{1}{\mathrm{NP}}\sum_{i=1}^{\mathrm{NP}}\frac{|k_{\mathrm{obs}}^{\mathrm{exp}}-k_{\mathrm{obs}}^{\mathrm{mod}}|}{k_{\mathrm{obs}}^{\mathrm{exp}}} \tag{23}$$

The obtained model can explain the observed data very well. However, the estimated value for b_{H_2O} leads to extremely low values for the exponential function, causing the estimated values for a_{H_2O} to be extremely high. The multiplication of the two factors give k_{H_2O} with magnitudes varying from 10^{-8} to 10^{0}, while the order of magnitude of k_{MAPA} varies is from 10^{-2} to 10^{0}.

At low temperatures, the water term contribution is not very significant, especially at low concentrations. This is reflected in the linearity observed in the Arrhenius plots (Figure 6). For 3 M and 4 M, the linear region goes up to 45°C, while at higher concentrations there is no linearity in the investigated temperature range. This is due to a large contribution form the water term, as shown in Figure 7. These results are better analyzed in Figure 7, which gives the contribution of the term for water as base, as defined by Eq. 24. For 5 M, the water term contribution is almost 90% at 60°C, and we can infer that at even higher temperatures and concentrations, the MAPA contribution would become negligible.

That the MAPA contribution becomes less important as its concentration increases may seem counterintuitive as the frequency of collisions between MAPA molecules would be expected to increase with concentration. This result could be only a numerical effect, due to the strong correlation between the regressed parameters, thus having no physical meaning. Conversely, aqueous MAPA solutions are extremely nonideal,[43] and the observed change in the behavior of the contributions of MAPA and water to the kinetics may be a consequence of changes in the solution structure. Within the 1 M to 5 M MAPA concentration range, the activity of MAPA increases more than 10 times with increasing concentration.[43] This difference may be due to different orientations of MAPA molecules

$$\%k_{H_2O}=\frac{a_{H_2O}\exp\left(\frac{b_{H_2O}}{T}\right)c_{H_2O}c_{MAPA}}{\left\{a_{MAPA}\exp\left(\frac{b_{MAPA}}{T}\right)c_{MAPA}+a_{H_2O}\exp\left(\frac{b_{H_2O}}{T}\right)c_{H_2O}\right\}c_{MAPA}} \tag{24}$$

The behavior of the alpha parameters as functions of concentration of MAPA can be observed in Figure 8. It is clear that the regressed α_{H_2O} parameter increase almost linearly with concentration. Its value spans from 59 to 67, a change of 8 units that, transformed back to a_{H_2O}, means a change of three orders of magnitude. The regressed α_{MAPA} parameters follow a second order polynomial with concentration. Its value spans from 13 to 15, a change of 2 units that, transformed back to a_{MAPA}, means a change of one order of magnitude.

To generalize the final correlation and as the regressed parameters were found to be highly correlated to the solution concentration, a new optimization was carried out, already incorporating the observed dependency when regressing the parameters. The expressions used for a_{MAPA} and a_{H_2O} are given in Eqs. 25 and 26. The new objective function to be minimized is presented in Eq. 27. In this new formulation, a total of seven parameters are regressed against all the experimental points available. The parameters are independent of both concentration and temperature. The optimum values are given in Table 5

$$a_{MAPA}=\exp\left[\beta_{MAPA}\left(\frac{c_{MAPA}}{1000}\right)^2+\gamma_{MAPA}\frac{c_{MAPA}}{1000}+\theta_{MAPA}\right] \tag{25}$$

$$a_{H_2O}=\exp\left(\gamma_{H_2O}\frac{c_{MAPA}}{1000}+\theta_{H_2O}\right) \tag{26}$$

$$\mathrm{Fobj}=\sum_{i=1}^{\mathrm{NP}}\frac{\left\{k_{\mathrm{obs}}(i)-\left\{\begin{array}{l}\exp\left[\beta_{MAPA}\left(\frac{c_{MAPA}(i)}{1000}\right)^2+\gamma_{MAPA}\frac{c_{MAPA}(i)}{1000}+\theta_{MAPA}+\frac{b_{MAPA}}{T}\right]c_{MAPA}(i)\\ +\exp\left(\gamma_{H_2O}\frac{c_{MAPA}(i)}{1000}+\theta_{H_2O}+\frac{b_{H_2O}}{T}\right)c_{H_2O}(i)\end{array}\right\}c_{MAPA}(i)\right\}^2}{u_{\mathrm{kobs}}^2(i)} \tag{27}$$

Attempts to simplify the expression in Eq. 25 by zeroing either β_{MAPA}, γ_{MAPA}, or both lead to large errors when predicting the observed kinetic constant. Using the expressions for a_{MAPA} and a_{H_2O} given in Eqs. 25 and 26 leads to acceptable errors, but somewhat higher than those obtained previously, as seen when comparing the errors reported in Table 4 with those in Table 6 and as shown in Figure 5. This result is of great importance because Eq. 27 can be applied for any concentration and temperature within the experimental data range. This simplifies the implementation of rate based models in process simulators, for instance.

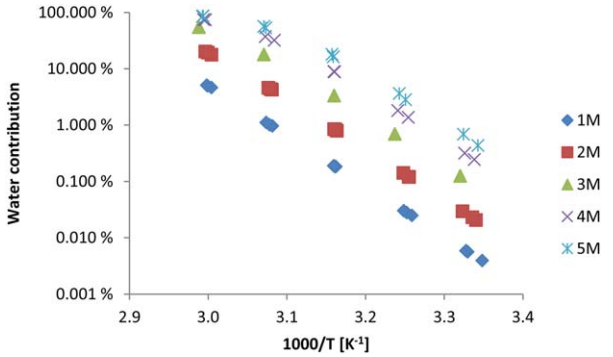

Figure 7. Contribution of the water term, as defined by Eq. 24.

[Color figure can be viewed in the online issue, which is available at wileyonlinelibrary.com.]

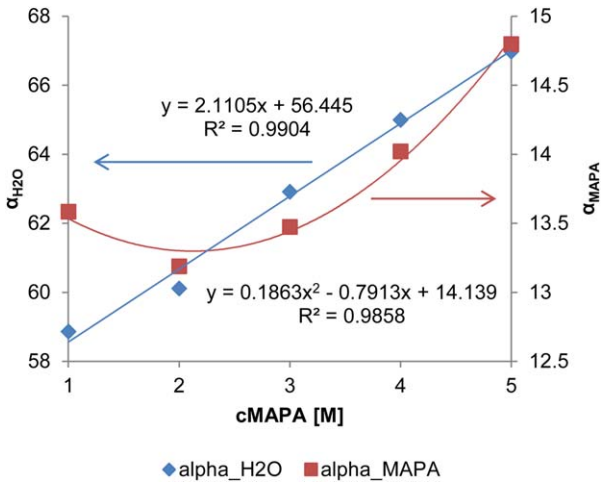

Figure 8. Correlation for parameter values as functions of MAPA concentration.

[Color figure can be viewed in the online issue, which is available at wileyonlinelibrary.com.]

It should also be kept in mind that errors in k_{obs} will translate by their square root when back-calculated into transfer fluxes, that is, 20% error in k_{obs} will give 10% error in mass transfer flux. The good agreement between the calculated and the experimentally determined CO_2 absorption fluxes can be observed in the parity plot presented in Figure 9, where all the points are between the $y = 0.9x$ and the $y = 1.1x$ lines.

Examples of joint confidence regions for the regressed parameters at a confidence level of 95% are given in Figure 10. During the optimization, the objective function was evaluated 600,000 times (5000 iterations, swarm size = 40, operation repeated three times; for further information see Monteiro et al.[42]). The points that compose the joint confidence regions are those which fulfil the relationship presented in inequality 28. This inequality is exact for linear models only, but provide a very good approximation of the confidence regions for nonlinear models.[40] It can be seen in

Table 6. Optimization Results Using Eq. 27

	Optimization Using Correlations	
MAPA Concentration	F_{obj}	ARD %
1 M	7.2	8.5
2 M	9.1	8.7
3 M	2.1	8.7
4 M	62	11.5
5 M	24.2	34.2

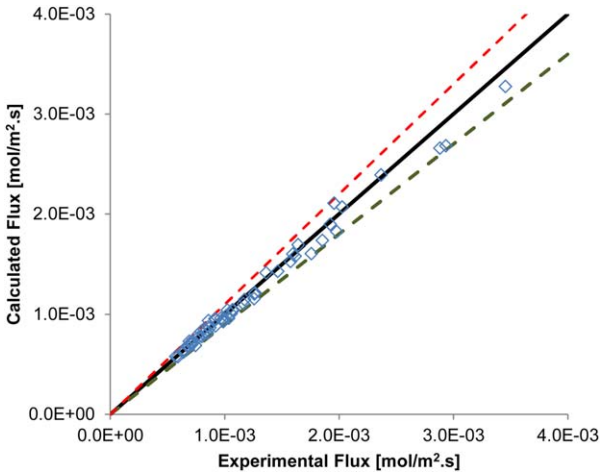

Figure 9. Parity plot for calculated vs. experimentally determined CO_2 absorption flux.

Black line: $y = x$; Red dashed line: $y = 1.1x$; Green dashed line: $y = 0.9x$. [Color figure can be viewed in the online issue, which is available at wileyonlinelibrary.com.]

Figure 10 that some parameters are strongly correlated to others. All the regressed parameters were found to be statistically significant

$$F_{obj}(\underline{\Theta}) \leq F_{obj}\left(\underline{\hat{\Theta}}\right)\left(1+\frac{p}{NP-p}F^{\sigma}_{p,NP-p}\right) \qquad (28)$$

The values obtained for a_{MAPA} and b_{MAPA} are within the range of known kinetic constants for the carbamate reaction in alkanolamine solutions reported in literature.[13,44] Moreover, the k_{obs} value for MAPA has the same order of magnitude as the k_{obs} for PZ calculated from the data presented by Bishnoi and Rochelle.[31] A third diamine, AEEA 2-(2-aminoethyl-amino)ethanol, is found to have a performance closer to that of MEA.[8] For comparison, these values are presented in Table 7 for 1 M solutions at 25°C.

Conclusions

The CO_2 absorption rate in unloaded MAPA aqueous solutions with concentrations varying between 1 M and 5 M were measured. The experimental temperature range was 25 to 60°C. Because MAPA is a fast absorbing system, the CO_2

Table 5. Parameters Regressed Using Eq. 27

Parameter	β_{MAPA}	γ_{MAPA}	θ_{MAPA}	b_{MAPA}	γ_{H_2O}	θ_{H_2O}	b_{H_2O}
Value	0.2092	−0.9437	12.5290	−4238.31	2.0041	64.9814	−24919.86

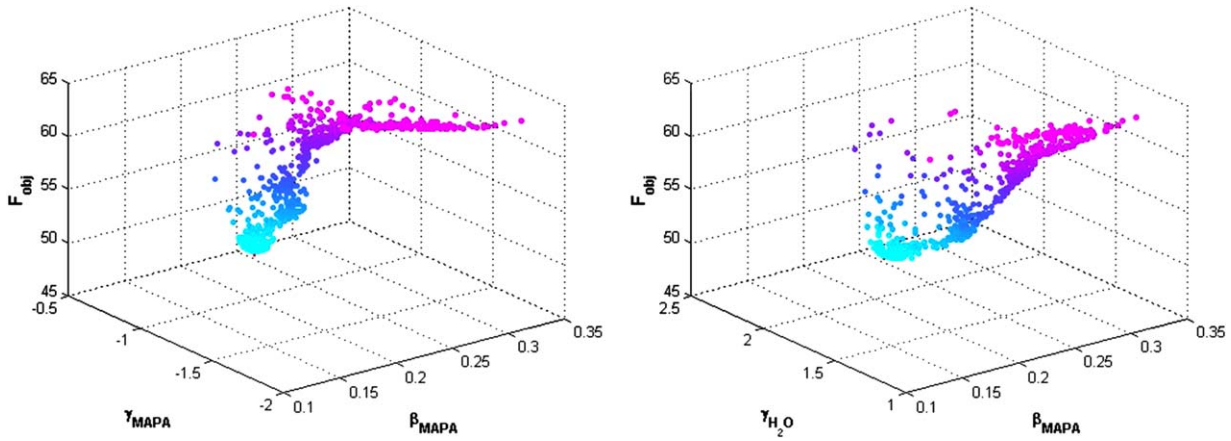

Figure 10. Example of joint confidence intervals for the estimated parameters.

[Color figure can be viewed in the online issue, which is available at wileyonlinelibrary.com.]

partial pressure was kept low, in the range of 0.1 to 0.3 kPa in the experiments performed in a string of discs contactor. Measurements for the 2 M MAPA solutions were performed in a wetted wall column for pressures from 2 to 13 kPa, and the obtained overall mass-transfer coefficients agree reasonably well with those obtained in the string of discs contactor.

All experiments were run on unloaded solutions. The reproducibility and repeatability of the experiments was found to be good. However, observed deviations between parallel evaluations of the overall mass-transfer coefficient were around 5%, a value significantly larger than uncertainties calculated based on uncertainties in instrumental and analytical procedures (around 1%), but still very satisfactory.

To obtain values for the observed kinetic constant, k_{obs} the experimental results were interpreted using a two-film mass-transfer model[17] and invoking the pseudo-first order assumption. Needed experimental values for density, viscosity, and Henry's law coefficient for CO_2 were measured and are given. The results indicate that MAPA is almost twice as fast as PZ, eight times faster than AEEA, and 15 times faster than MEA, when comparing unloaded 1 M solutions at 25°C.

The observed kinetic constant was modeled using the direct mechanism,[21] considering both water and MAPA as possible proton receivers. The observed kinetic constants of the model were unfolded using the Arrhenius representation, and the pre-exponential and energy parameters were regressed using the PSO algorithm.[39]

Very good agreement was obtained between the experimental data and the model, indicating that the direct mechanism can explain the MAPA carbamate formation reaction. However, the estimated pre-exponential parameter values for representing the reaction when water is the proton receiver were unreasonably high and a reparameterization was applied to avoid numerical imprecisions which arise when computing large numbers.

The final expression for k_{obs} can be applied for any concentration and temperature within the experimental data range, and, together with the presented physical data, comprises a complete model for calculating absorption fluxes.

Table 7. Kinetic Values Observed for Diamines and MEA, for 1 M Solutions at 25°C

Amine	k_{obs} (s^{-1})	Source
MAPA	9.65E4	This work
PZ	5.37E4	Bishnoi and Rochelle (2000)
AEEA	1.21E4	Ma'mun et al. (2006)
MEA	6.00E3	Versteeg et al. (1996)

Acknowledgments

Financial support from the EC 7th Framework Programme through Grant Agreement No: iCap-241391, is gratefully acknowledged

Literature Cited

1. Chen X, Closmann F, Rochelle GT. Accurate screening of amines by the wetted wall column. *Energy Procedia*. 2011;4(0):101–108.
2. Brúder P, Svendsen HF. Capacity and kinetics of solvents for post-combustion CO_2 capture. *Energy Procedia*. 2012;23(0):45–54.
3. Brúder P, Owrang F, Svendsen HF. Pilot study—CO2 capture into aqueous solutions of 3-methylaminopropylamine (MAPA) activated dimethyl-monoethanolamine (DMMEA). *Int J Greenhouse Gas Control*. 2012;11(0):98–109.
4. Liebenthal U, Pinto DDD, Monteiro JGM-S, Svendsen HF, Kather A. Overall process analysis and optimisation for CO_2 capture from coal fired power plants based on phase change solvents forming two liquid phases. *Energy Procedia*. 2013;37:1844–1854.
5. Mangalapally HP, Notz R, Asprion N, Sieder G, Garcia H, Hasse H. Pilot plant study of four new solvents for post combustion carbon dioxide capture by reactive absorption and comparison to MEA. *Int J Greenhouse Gas Control*. 2012;8(0):205–216.
6. Zhicheng X, Shujuan W, Bo Z, Changhe C. Study on potential biphasic solvents: absorption capacity, CO2 loading and reaction rate. *Energy Procedia*. 2013;37(0):494–498.
7. Stephens EJ, Morris GA. Determination of liquid-film absorption coefficients. *Chem Eng Prog*. 1951;47(5):11.
8. Ma'mun S, Dindore VY, Svendsen HF. Kinetics of the reaction of carbon dioxide with aqueous solutions of 2-((2-aminoethyl)amino) ethanol. *Ind Eng Chem Res*. 2006;46(2):385–394.
9. Knuutila H, Svendsen HF, Juliussen O. Kinetics of carbonate based CO2 capture systems. *Energy Procedia*. 2009;1(1):1011–1018.
10. Hartono A, Svendsen HF. Kinetics reaction of primary and secondary amine group in aqueous solution of diethylenetriamine (DETA) with carbon dioxide. *Energy Procedia*. 2009;1(1):853–859.
11. Luo X, Hartono A, Svendsen HF. Comparative kinetics of carbon dioxide absorption in unloaded aqueous monoethanolamine solutions using wetted wall and string of discs columns. *Chem Eng Sci*. 2012; 82(0):31–43.
12. Versteeg GF, van Swaaij WPM. Solubility and diffusivity of acid gases (carbon dioxide, nitrous oxide) in aqueous alkanolamine solutions. *J Chem Eng Data*. 1988;33(1):29–34.
13. Versteeg GF, Van Dijck LAJ, Van Swaaij WPM. On the kinetics between CO2 and alkanolamines both in aqueous and non-aqueous solutions. *An overview. Chem Eng Commun*. 1996;144:113–158.
14. Hartono A, Mba EO, Svendsen HF. Physical properties of partially CO_2 loaded aqueous monoethanolamine (MEA). *J Chem Eng Data*. 2014;59(6):1808–1816.

15. Pinto DDD, Monteiro JGMS, Johnsen B, Svendsen HF, Knuutila H. Density measurements and modelling of loaded and unloaded aqueous solutions of MDEA (N-methyldiethanolamine), DMEA (N,N-dimethylethanolamine), DEEA (diethylethanolamine) and MAPA (N-methyl-1,3-diaminopropane). *Int J Greenhouse Gas Control*. 2014; 25(0):173–185.
16. Knuutila H, Juliussen O, Svendsen HF. Density and N2O solubility of sodium and potassium carbonate solutions in the temperature range 25 to 80 °C. *Chem Eng Sci*. 2010;65(6):2177–2182.
17. Danckwerts PV. *Gas-Liquid Reactions*. New York: McGraw Hill, 1985.
18. Meyer VR. Measurement uncertainty. *J Chromatogr A*. 2007; 1158(1–2):15–24.
19. Ciftja AF, Hartono A, Svendsen HF. Experimental study on phase change solvents in CO2 capture by NMR spectroscopy. *Chem Eng Sci*. 2013;102(0):378–386.
20. Danckwerts PV. The reaction of CO2 with ethanolamines. *Chem Eng Sci*. 1979;34(4):443–446.
21. Crooks JE, Donnellan JP. Kinetics and mechanism of the reaction between carbon dioxide and amines in aqueous solution. *J Chem Soc Perkin Trans 2*. 1989;0(4):331–333.
22. da Silva EF, Svendsen HF. Ab initio study of the reaction of carbamate formation from CO2 and alkanolamines. *Ind Eng Chem Res*. 2004;43(13):3413–3418.
23. Shim J-G, Kim J-H, Jhon YH, Kim J, Cho K-H. DFT Calculations on the role of base in the reaction between CO2 and monoethanolamine. *Ind Eng Chem Res*. 2009;48(4):2172–2178.
24. Arstad B, Blom R, Swang O. CO2 Absorption in aqueous solutions of alkanolamines: mechanistic insight from quantum chemical calculations. *J Phys Chem A*. 2007;111(7):1222–1228.
25. Gibson KD. True and apparent activation energies of enzymic reactions. *Biochim Biophys Acta*. 1953;10(2):221–229.
26. Schwaab M, Pinto JC. Optimum reference temperature for reparameterization of the Arrhenius equation. Part 1: problems involving one kinetic constant. *Chem Eng Sci*. 2007;62(10):2750–2764.
27. da Silva EF, Kuznetsova T, Kvamme B, Merz KM. Molecular dynamics study of ethanolamine as a pure liquid and in aqueous solution. *J Phys Chem B*. 2007;111(14):3695–3703.
28. Han B, Zhou C, Wu J, Tempel DJ, Cheng H. Understanding CO2 capture mechanisms in aqueous monoethanolamine via first principles simulations. *J Phys Chem Lett*. 2011;2(6):522–526.
29. Han B, Sun Y, Fan M, Cheng H. On the CO2 capture in water-free monoethanolamine solution: an ab initio molecular dynamics study. *J Phys Chem B*. 2013;117(19):5971–5977.
30. Hartono A, da Silva EF, Svendsen HF. Kinetics of carbon dioxide absorption in aqueous solution of diethylenetriamine (DETA). *Chem Eng Sci*. 2009;64(14):3205–3213.
31. Bishnoi S, Rochelle GT. Absorption of carbon dioxide into aqueous piperazine: reaction kinetics, mass transfer and solubility. *Chem Eng Sci*. 2000;55(22):5531–5543.
32. Kim I. Heat of Reaction and VLE of Post Combustion CO2 Absorbents. Trondheim, Norway: PhD Thesis. Faculty of Natural Sciences and Technology, Department of Chemical Engineering, Norwegian University of Science and Technology, NTNU; 2009:50.
33. Levenspiel O. Chemical Reaction Engineering, 3rd ed., John Wiley & Sons, New York, 1999.
34. Brauner N, Shacham M. Statistical analysis of linear and nonlinear correlation of the Arrhenius equation constants. *Chem Eng Process: Process Intensification*. 1997;36(3):243–249.
35. Curl RL. Letters to the editor. *AIChE J*. 1993;39(8):1420–1420.
36. Sundberg R. Statistical aspects on fitting the Arrhenius equation. *Chemometr Intell Lab Syst*. 1998;41(2):249–252.
37. Chen NH, Aris R. Determination of Arrhenius constants by linear and nonlinear fitting. *AIChE J*. 1992;38(4):626–628.
38. Klicka R, Kubácek L. Statistical properties of linearization of the Arrhenius equation via the logarithmic transformation. *Chemometr Intell Lab Syst*. 1997;39(1):69–75.
39. Kennedy J, Eberhart R. Particle Swarm Optimization. In: Proceedings of IEEE International Conference on Neural Networks, vol. 4, pp. 1942–1948, Nov/Dec 1995.
40. Schwaab M, Biscaia JEC, Monteiro JL, Pinto JC. Nonlinear parameter estimation through particle swarm optimization. *Chem Eng Sci*. 2008;63(6):1542–1552.
41. Poli R, Kennedy J, Blackwell T. Particle swarm optimization. *Swarm Intell*. 2007;1(1):33–57.
42. Monteiro JGMS, Pinto DDD, Zaidy SAH, Hartono A, Svendsen HF. VLE data and modelling of aqueous N,N-diethylethanolamine (DEEA) solutions. *Int J Greenhouse Gas Control*. 2013;19(0):432–440.
43. Hartono A, Saleem F, Arshad MW, Usman M, Svendsen HF. Binary and ternary VLE of the 2-(diethylamino)-ethanol (DEEA)/3-(methylamino)-propylamine (MAPA)/water system. *Chem Eng Sci*. 2013; 101(0):401–411.
44. Vaidya PD, Kenig EY. CO2-Alkanolamine reaction kinetics: a review of recent studies. *Chem Eng Technol*. 2007;30(11):1467–1474.

Appendix

Table A1. Experimental Data and Calculation Results for MAPA 1 M Solutions

Experiment	T [°C]	ρ [kg m^{-3}]	μ [Pa s]	H_{CO_2} [Pa m^3 mol^{-1}]	$P^v_{solution}$ [kPa]	K_{ov} [mol m^{-2} kPa^{-1} s^{-1}]	k_G [mol m^{-2} kPa^{-1} s^{-1}]	k_L [m s^{-1}]	k_{obs} [s^{-1}]	E
1M a	27.39	989.7	1.29E-03	3449	3.61	2.92E-03	1.48E-02	1.26E-02	1.08E+05	2.10E+02
9.08 wt %	34.69	987.0	1.09E-03	4014	5.47	3.17E-03	1.46E-02	1.62E-02	1.51E+05	2.33E+02
07.07.2011	43.36	983.2	9.09E-04	4695	8.71	3.48E-03	1.45E-02	2.15E-02	2.14E+05	2.53E+02
	52.20	978.9	7.75E-04	5539	13.59	3.76E-03	1.44E-02	2.82E-02	3.07E+05	2.80E+02
	60.30	974.5	6.86E-04	6441	19.95	4.24E-03	1.35E-02	3.98E-02	5.24E+05	3.43E+02
1M b	27.18	989.7	1.30E-03	3427	3.56	2.82E-03	1.50E-02	1.19E-02	9.77E+04	2.03E+02
9.08 wt %	34.34	987.1	1.11E-03	3980	5.36	3.06E-03	1.48E-02	1.54E-02	1.37E+05	2.22E+02
08.07.2011	43.20	983.3	9.12E-04	4677	8.63	3.37E-03	1.46E-02	2.05E-02	1.96E+05	2.42E+02
	51.74	979.1	7.79E-04	5502	13.29	3.49E-03	1.45E-02	2.53E-02	2.49E+05	2.54E+02
	60.41	974.8	6.92E-04	6368	20.06	4.00E-03	1.30E-02	3.67E-02	4.49E+05	3.24E+02
1M c	25.53	990.3	1.35E-03	3289	3.24	2.87E-03	1.56E-02	1.16E-02	9.65E+04	2.08E+02
8.91 wt %	33.72	987.4	1.12E-03	3935	5.18	3.19E-03	1.55E-02	1.58E-02	1.47E+05	2.34E+02
05.02.2013	43.11	983.4	9.16E-04	4660	8.60	3.56E-03	1.53E-02	2.16E-02	2.19E+05	2.67E+02
	51.37	979.2	7.82E-04	5474	13.05	3.91E-03	1.49E-02	2.91E-02	3.30E+05	3.02E+02
	59.75	975.0	6.95E-04	6338	19.47	4.14E-03	1.32E-02	3.83E-02	4.91E+05	3.48E+02

Table A2. Experimental Data and Calculation Results for MAPA 2 M Solutions

Experiment	T [°C]	ρ [kg m^{-3}]	μ [Pa s]	H_{CO_2} [Pa m^3 mol^{-1}]	$P^v_{solution}$ [kPa]	K_{ov} [mol m^{-2} kPa^{-1} s^{-1}]	k_G [mol m^{-2} kPa^{-1} s^{-1}]	k_L [m s^{-1}]	k_{obs} [s^{-1}]	E
2M a	27.78	985.3	1.95E-03	3761	3.62	3.53E-03	1.50E-02	1.74E-02	2.87E+05	5.84E+02
18.27 wt %	34.06	982.2	1.63E-03	4258	5.18	3.75E-03	1.48E-02	2.14E-02	3.62E+05	6.12E+02
06.07.2011	43.31	977.5	1.29E-03	4934	8.52	4.24E-03	1.46E-02	2.94E-02	5.35E+05	6.69E+02
	51.65	972.8	1.07E-03	5556	12.98	4.52E-03	1.45E-02	3.66E-02	6.70E+05	7.02E+02
	60.63	967.5	9.04E-04	6401	19.89	5.23E-03	1.31E-02	5.57E-02	1.28E+06	9.20E+02
2M b	26.25	985.7	2.02E-03	3682	3.31	3.52E-03	1.53E-02	1.68E-02	2.79E+05	5.86E+02
18.27 wt %	34.09	982.2	1.63E-03	4258	5.19	3.91E-03	1.49E-02	2.26E-02	4.03E+05	6.41E+02
10.07.2011	42.96	977.7	1.30E-03	4913	8.37	4.46E-03	1.50E-02	3.12E-02	6.05E+05	7.23E+02
	51.93	972.6	1.07E-03	5577	13.16	5.02E-03	1.47E-02	4.26E-02	9.03E+05	8.18E+02
	59.73	967.6	9.05E-04	6402	19.09	5.29E-03	1.38E-02	5.50E-02	1.25E+06	9.25E+02
2M c	26.64	985.6	2.01E-03	3696	3.39	3.40E-03	1.58E-02	1.60E-02	2.52E+05	5.56E+02
18.03 wt %	34.74	982.0	1.62E-03	4278	5.38	3.90E-03	1.59E-02	2.21E-02	3.82E+05	6.18E+02
06.03.2013	43.15	977.7	1.30E-03	4895	8.46	4.48E-03	1.56E-02	3.08E-02	5.91E+05	7.03E+02
	51.42	972.9	1.08E-03	5525	12.85	5.11E-03	1.54E-02	4.23E-02	9.01E+05	8.12E+02
	60.26	967.8	9.10E-04	6360	19.57	5.58E-03	1.35E-02	6.03E-02	1.51E+06	1.02E+03

Table A3. Experimental Data and Calculation Results for MAPA 3 M Solutions

Experiment	T [°C]	ρ [kg m^{-3}]	μ [Pa s]	H_{CO_2} [Pa m^3 mol^{-1}]	$P^v_{solution}$ [kPa]	K_{ov} [mol m^{-2} kPa^{-1} s^{-1}]	k_G [mol m^{-2} kPa^{-1} s^{-1}]	k_L [m s^{-1}]	k_{obs} [s^{-1}]	E
3M	28.04	981.9	3.18E-03	4370	3.59	4.11E-03	1.61E-02	2.41E-02	8.14E+05	8.75E+02
27.18 wt %	35.77	977.5	2.50E-03	4801	5.57	4.73E-03	1.55E-02	3.26E-02	1.17E+06	9.79E+02
07.03.2013	43.31	972.6	1.98E-03	5263	8.34	5.51E-03	1.55E-02	4.49E-02	1.75E+06	1.09E+03
	52.53	966.2	1.53E-03	5788	13.27	6.55E-03	1.52E-02	6.67E-02	2.95E+06	1.21E+03
	61.51	960.2	1.26E-03	6330	20.27	7.73E-03	1.43E-02	1.07E-01	6.06E+06	1.57E+03

Table A4. Experimental Data and Calculation Results for MAPA 4 M Solutions

Experiment	T [°C]	ρ [kg m^{-3}]	μ [Pa s]	H_{CO_2} [Pa m^3 mol^{-1}]	$P^v_{solution}$ [kPa]	K_{ov} [mol m^{-2} kPa^{-1} s^{-1}]	k_G [mol m^{-2} kPa^{-1} s^{-1}]	k_L [m s^{-1}]	k_{obs} [s^{-1}]	E
4M a 36.76 wt %	26.43	979.3	5.50E-03	4956	3.17	4.75E-03	1.51E-02	3.44E-02	2.59E+06	2.16E+03
30.06.2011	34.15	973.8	4.11E-03	5279	4.94	5.23E-03	1.49E-02	4.26E-02	3.00E+06	1.98E+03
	43.35	967.2	2.97E-03	5590	8.11	6.73E-03	1.47E-02	6.95E-02	5.80E+06	2.37E+03
	52.31	960.3	2.24E-03	5859	12.75	8.38E-03	1.47E-02	1.14E-01	1.16E+07	2.81E+03
	60.86	953.5	1.76E-03	6138	19.12	9.98E-03	1.36E-02	2.30E-01	3.70E+07	4.66E+03
4M b 36.15 wt %	27.52	979.2	5.46E-03	4951	3.38	4.91E-03	1.62E-02	3.50E-02	2.65E+06	2.15E+03
08.02.2013	35.42	973.5	4.04E-03	5289	5.31	6.05E-03	1.61E-02	5.13E-02	4.26E+06	2.18E+03
	43.26	967.3	2.98E-03	5585	8.08	6.76E-03	1.59E-02	6.57E-02	5.20E+06	2.03E+03
	51.13	961.0	2.29E-03	5838	12.04	8.21E-03	1.56E-02	1.01E-01	9.41E+06	2.36E+03
	60.57	954.1	1.79E-03	6111	18.89	9.86E-03	1.43E-02	1.94E-01	2.67E+07	3.95E+03

Table A5. Experimental Data and Calculation Results for MAPA 5 M Solutions

Experiment	T [°C]	ρ [kg m^{-3}]	μ [Pa s]	H_{CO_2} [Pa m^3 mol^{-1}]	$P^v_{solution}$ [kPa]	K_{ov} [mol m^{-2} kPa^{-1} s^{-1}]	k_G [mol m^{-2} kPa^{-1} s^{-1}]	k_L [m s^{-1}]	k_{obs} [s^{-1}]	E
5M a 46.35 wt %	26.03	973.5	9.28E-03	5093	2.98	6.02E-03	1.53E-02	5.05E-02	8.54E+06	5.12E+03
30.06.2011	34.48	966.6	6.34E-03	5274	4.84	7.17E-03	1.49E-02	7.27E-02	1.24E+07	5.10E+03
	43.44	959.1	4.30E-03	5350	7.84	8.28E-03	1.50E-02	9.91E-02	1.59E+07	4.67E+03
	52.27	951.6	3.05E-03	5459	12.25	1.06E-02	1.46E-02	2.09E-01	5.05E+07	6.98E+03
	61.01	944.0	2.24E-03	5643	18.56	1.29E-02	1.35E-02	1.57E+00	2.08E+09	3.93E+04
5M b 44.07 wt %	27.68	972.9	8.92E-03	5099	3.32	6.50E-03	1.67E-02	5.42E-02	9.44E+06	4.80E+03
09.02.2013	35.25	966.2	6.19E-03	5276	5.10	7.45E-03	1.59E-02	7.39E-02	1.25E+07	4.76E+03
	43.59	959.1	4.30E-03	5349	7.99	9.10E-03	1.55E-02	1.18E-01	2.24E+07	5.69E+03
	52.51	951.5	3.04E-03	5458	12.52	1.12E-02	1.51E-02	2.36E-01	6.39E+07	8.14E+03
	60.92	944.2	2.25E-03	5635	18.66	1.24E-02	1.41E-02	5.93E-01	3.00E+08	1.49E+04

Manuscript received Mar. 2, 2014, and revision received June 4, 2014.